Int. J. Electrochem. Sci., 15 **(2020)** 8422 – 8436, doi: 10.20964/2020.09.71

International Journal of
ELECTROCHEMICAL
SCIENCE
www.electrochemsci.org

Effects of Pressure Evolution on the Decrease in the Capacity of Lithium-Ion Batteries

Jun Zhang[1], *Bowen Kang*[1,*], *Qing Luo*[2] , *Shunzhang Zou*[1]

[1] College of Mechanical and Vehicle Engineering, Hunan University, Changsha 410082, Hunan, China
[2] Hunan Fengyuan Yeshine Kingco New Energy Co., Ltd., Changsha 410100, Hunan, China
Corresponding author: Kang Bowen
[*]E-mail: kbw520@hnu.edu.cn

Received: 2 June 2020 / *Accepted:* 15 July 2020 / *Published:* 10 August 2020

External mechanical pressure can affect the cycle life of lithium-ion battery. In this paper, the evolution process of the mechanical pressure that a lithium-ion battery was subjected to during approximately 3000 cycles under the fixed constraint was studied through charge-discharge cycling tests of a lithium-ion battery. The effect of external pressure on battery aging in the late cycle stage was explored through SEM and incremental capacity analysis (ICA). In addition, three groups of comparative experiments, including a rigid constraint, an elastic silicone pad constraint and a spring constraint, were set up to explore the influence of different constraint schemes on battery cycle life. The experimental results showed that the mechanical pressure increased due to the aging of the battery under the fixed constraint, which could cause the anode material of the battery to crack. In the comparative experiment, the capacity decrease rate of the spring compression constraint scheme was 5.13% and 6.17% lower than those of the other two groups. The ohmic resistance increase rate was 8.67% and 12.36% lower than those of the other two groups, and the coulombic efficiency of the spring constraint remained good in the late stage of the cycle. Therefore, the spring constraint scheme can maximize the positive effect of external pressure on lithium-ion batteries by maintaining a relatively stable external pressure. The results presented in this paper have a certain guiding significance for the design of the battery pack.

Keywords: lithium-ion battery; pressure evolution; aging; decrease in capacity

1. INTRODUCTION

The widespread use of fossil fuels in industrial equipment and transportation contributes to environmental pollution and global warming. Moreover, they are nonrenewable resources, and their energy utilization efficiency is still relatively low. Today, lithium-ion batteries are widely used in electric vehicles and energy storage devices because of their high specific energy and high efficiency [1]. However, with the increasing demand for equipment, these applications engender higher

requirements for battery performance and cycle life. Accordingly, extensive studies have been conducted on the aging mechanisms of lithium-ion batteries, such as formation and growth of the solid electrolyte interphase (SEI) film, lithium plating, and degradation of the composite electrode assembly [2-8]. These materials science and electrochemistry studies have taken into account the effects of different environmental and usage conditions, such as the depth of discharge, charge and discharge states, charge and discharge rates, and temperature, on battery aging. However, compared with these factors, the external pressure as an important factor of battery aging is less studied.

The external pressure on a battery stems from the rigid constraints imposed on the battery, particularly the rigid container that keeps the battery immobile and prevents it from vibrating during use. Owing to the physical constraints of their external casings and the fact that they continuously undergo volume changes during charge-discharge cycling, batteries are subjected to changes in pressure. Setting the optimal initial pressure is important because it could affect the performance and cycle life of batteries [9-13]. Although the initial before batteries are used pressure can be controlled, the pressure inside them gradually changes as they age. Currently, large lithium-ion batteries that feature electrode materials with high volume expansion rates, such as silicon, are increasingly used. Because batteries undergo large deformation during their charge-discharge cycles, it is increasingly important to investigate the effects of pressure evolution on battery performance.

Changes in external pressure manifest as changes in stress in batteries. Previous studies on battery stress mainly focused on electrode particles and planes and mostly relied on experimental or modeling approaches to investigate the effects of changes in the internal stress on the overall battery performance in the absence of external constraints [14-17]. Later, the stress caused by mechanical compression was considered in recent studies. Peabody and Arnold [18] determined that mechanical stress could cause separator deformation. Even if the stress level was as low as 0.1 MPa, it would still have a measurable effect on the capacity and internal resistance of batteries. Gnanaraj et al. [19] investigated the effects of the rolling process during battery manufacturing on electrode materials and reported that unlike rolled cathodes, rolled graphite anodes presented poor electrochemical performance. Barai et al. [9] and Mussa et al. [13] determined that batteries exposed to different pressure levels presented different cycling characteristics. Gert Berckmans et al. [20] reported that the application of external pressure leads to a significant increase in capacity of 19% and a significant decrease in discharge ohmic resistance of 50%, but their results showed that the initial applied pressure has little impact on the cell performance and lifetime. Verena Müller et al. [21] performed much research on external pressure and found an improved electrical contact resistance in compressed cells but an increased charge transfer resistance compared to uncompressed cycled cells.

Previous studies on the effects of the external pressure on battery aging have mainly focused on controlling the initial pressure. However, batteries undergo irreversible volume expansion during cycling, which causes the pressure to increase. Verena Müller et al. [22] studied the pressurizing methods in another paper, but they tested only one battery, which is different from the practical use of a battery pack. Few reports have been published on the effects of pressure evolution instead of initial pressure on battery aging to date or on the pressurization modes of battery packs.

This study aimed to analyze the effects of mechanical pressure evolution on battery aging under the fixed constraint by measuring the changes in external pressure on the surface of soft package

lithium-ion batteries and disassembling aging batteries. First, pressure sensor data at different positions on the surface of lithium-ion batteries were collected to reveal the pressure evolution patterns during individual charge-discharge cycles as well as the entire battery life. Then, the batteries were disassembled when their initial capacity decreased by 20%, the morphologies of the cathode and anode surfaces were observed by scanning electron microscopy (SEM), and the effects of the increase in pressure were analyzed. Last, different constraint modes were compared experimentally, and the results indicated that batteries that operated steadily under optimal pressure throughout their life cycles presented longer life cycles than those that operated under gradually increasing pressure.

2. EXPERIMENTAL

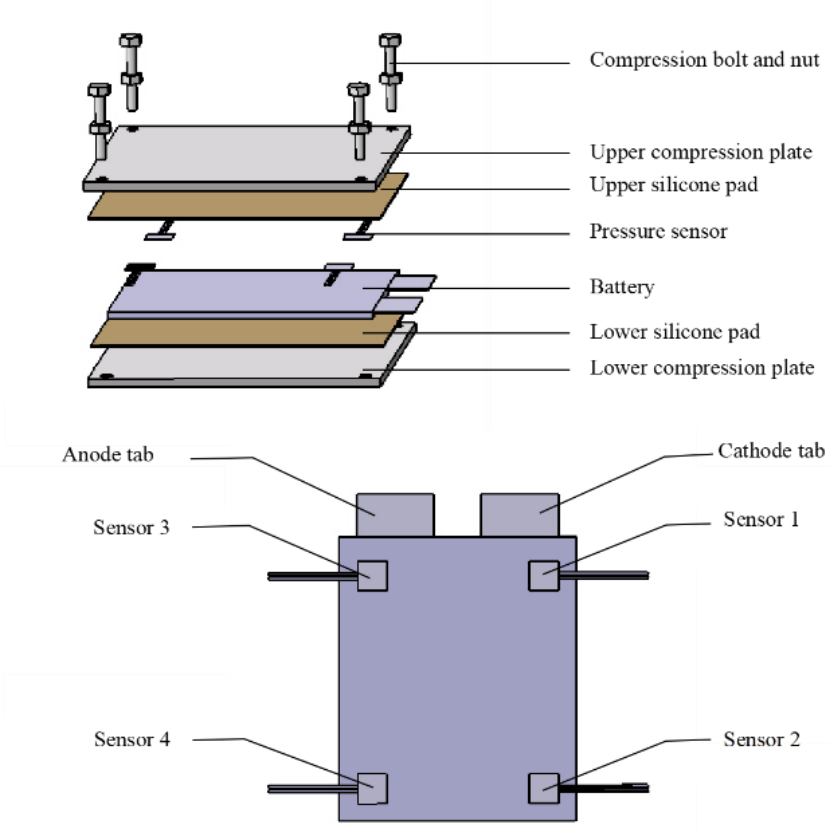

Figure 1. Schematic diagram of the pressurizing device and sensor setup.

A type of commercially available, soft package lithium-ion battery with a ternary cathode material was used in this study. The cathode and anode consisted of Li(Ni1/3Mn1/3Co1/3)O2 and graphite, respectively. The battery was composed of 16 cathode plates and 17 anode plates, fabricated by a lamination process, and LiPF6 was used as the electrolyte. The capacity of the battery was 37 Ah, and its nominal size was 269 mm × 212 mm × 7.4 mm. In one of our previous studies on optimization of the initial external pressure, we revealed that when the lithium-ion batteries were operated under an initial external pressure of 69 kPa (1000 N), they exhibited excellent charge-discharge cycling performance, and therefore, the pressure of 69 kPa was adopted as the initial pressure in this study [23].

The experimental setup is illustrated in Fig. 1.

To exert pressure uniformly on the large battery in this study, four thin-film pressure sensors were placed near the compression bolts, and silicone pads were placed between the steel compression plates and battery to minimize the effect of the uneven surface of the compression plates. The external pressure provided by the compression bolts and steel compression plates was used to simulate the actual pressure on the modules of the battery. Because the Young's modulus of steel is large, the deformation of the steel plates was negligible. Another battery of the same type was operated in the absence of constraints during its charge-discharge cycling as a control. The expansion of the battery due to temperature rise was ignored here because the experiment was operated at constant room temperature and the charge-discharge rate was relatively small.

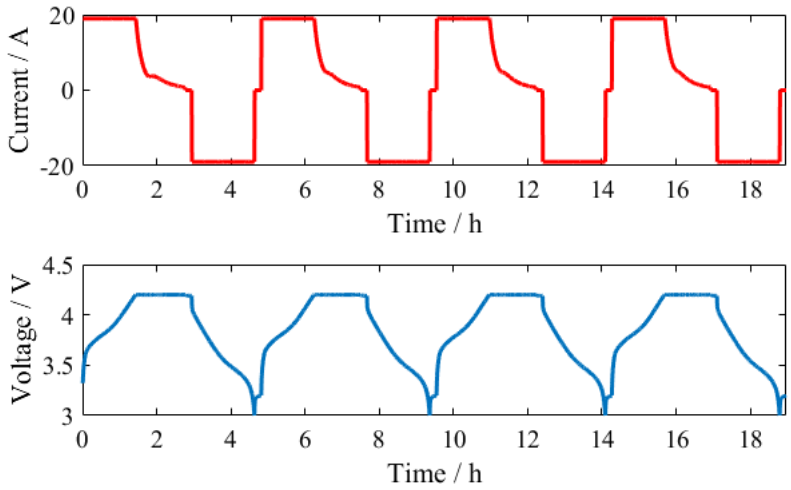

Figure 2. Curves of current and voltage vs. time

The batteries were subjected to constant-current constant-voltage charging and constant-current discharging, where the charge-discharge rate, upper cutoff voltage, and lower cutoff voltage were 0.5 C, 4.2 V, and 3.0 V, respectively, and the time interval between charging and discharging during a cycle was 10 min. The current and voltage curves are shown in Fig. 2. The thin-film pressure sensors converted the pressure signals into electrical signals, and the pressure changes on the battery surface were obtained by measuring the resistance of the sensors. Pressure measurements were conducted weekly when the batteries were discharged to the cutoff voltage, and the pressure changes on the battery surface were recorded. During this period, a cycle was randomly selected, and the pressure change with state of charge (SOC) in one cycle was completely recorded. Batteries were considered to have reached the end of their lives when their initial capacities decreased by 20%. Afterward, the aging batteries were disassembled in a dry, ventilated environment, and the electrode material was subjected to surface monitoring and failure analysis by using scanning electron microscopy (SEM).

3. RESULTS AND DISCUSSION

3.1 Evolution pattern of mechanical pressure

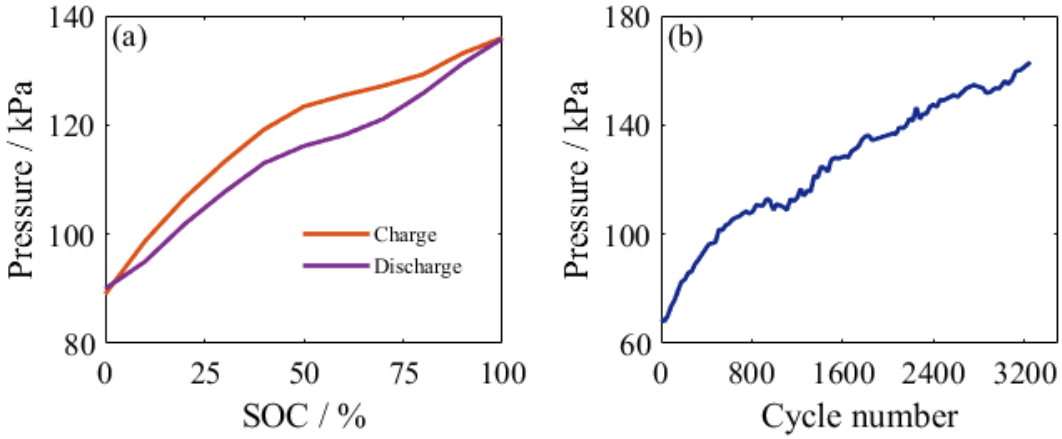

Figure 3. Pressure evolution curves: (a) pressure evolution with state of charge (SOC) during one charge-discharge cycle, and (b) average pressure of the four sensors vs. cycle number.

To investigate the pressure evolution during a single cycle, the pressure on the battery during a cycle in the early stage was measured over time. Fig. 3 (a) illustrates the average pressure evolution of the four sensors with state of charge (SOC) during a charge-discharge cycle, where the pressure on the battery gradually increased during charging and gradually decreased during discharging. This was mainly attributed to lithium ions being embedded in the graphite anode during charging, which caused the battery to expand, and to the lithium ions being released from the graphite anode during discharging, which caused the battery to shrink [16]. By contrast, the effects of embedding and releasing of lithium ions in the cathode on the battery volume were negligible [24]. The sensors indicated that the pressure increased when the silicone pads were compressed due to expansion of the battery. This meant that the more the volume expanded, the greater the pressure was. The pressure varied nonlinearly during cycles because lithium ions underwent phase changes when they were embedded in the anode, forming LiC_6. During the migration of lithium ions from the carbon-poor to carbon-rich areas, each phase underwent a transition and exhibited different expansion characteristics, as documented in detail in the literature [25, 26]. The pressure changes during a single charge-discharge cycle were noticeable, and the maximum pressure during a single cycle was approximately 1.5 times the minimum pressure.

Fig. 3 (b) presents the curve of the average pressure of the four sensors vs. cycle number throughout the life cycle of the battery. The pressure constantly increased during charging-discharging, which coincided with the irreversible expansion of the battery during use. The irreversible increase in pressure could be attributed to the structural change the anode material underwent, growth of the SEI film, gas generation and lithium plating during battery use [11, 27, 28]. However, the anode material structural change and lithium plating usually occur in the late stage of the cycle life or under extreme conditions such as a low temperature. Therefore, growth of the SEI film was considered to be the main reason for the irreversible increase in pressure in this paper. The SEI film contained inorganic components such as Li_2CO_3, and it would react with the HF generated by electrolytic decomposition to

produce CO_2 [8]. The growth of the SEI was accompanied by the side reaction producing the gas, so we treated the side reaction as part of SEI growth in the following. Owing to the growth of the SEI film, stress gradually accumulated in the electrode material, particularly in the anode. Although the initial pressure on the battery was relatively low, the battery was subjected to relatively high pressure during later charge-discharge cycles owing to battery expansion, which resulted from the irreversible accumulation of stress, and the pressure more than doubled during later charge-discharge cycles compared to the initial pressure.

3.2 Cause analysis of the decrease in capacity

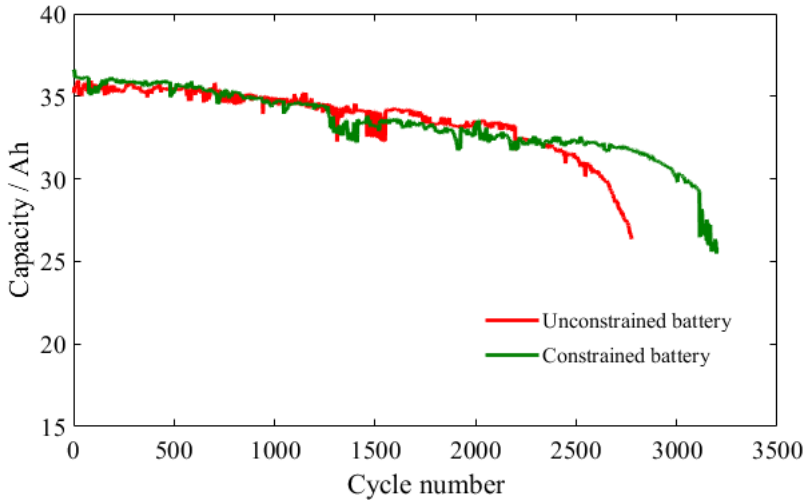

Figure 4. Decrease in capacity of constrained and unconstrained batteries.

Irreversible side reactions occur in batteries during charge-discharge cycling. These reactions consume the recyclable lithium and electrolyte in the batteries and consequently gradually decrease their capacity. Formation and growth of the SEI film are considered to be the key steps during this process [7]. The SEI film is a passivation layer that forms between the electrolyte and electrode material. It protects the electrode material and prevents it from further reacting with the electrolyte. While the SEI film formed on both the anode and cathode, the anode SEI film was typically analyzed because its effect on battery performance was greater than that of the cathode SEI film. The SEI film was typically formed during the first charge-discharge cycle. However, it continued to grow during subsequent cycles. Fig. 4 presents the decrease in the capacity of constrained and unconstrained batteries. As illustrated in Fig. 4, the capacity of the analyzed constrained and unconstrained batteries gradually decreased during approximately the first 2100 and 2500 charge-discharge cycles, respectively, which indicated that the internal environment of the batteries was relatively stable.

The cycle life of the constrained battery was longer than that of the unconstrained battery (Fig. 4). If a decrease in capacity of 20% is considered to represent the end of battery life, then the constrained battery operated for approximately 400 more charge-discharge cycles than the unconstrained one, and therefore, the cycle life of the constrained battery was 12.5% longer than that of the unconstrained one. Longer cycle lives are beneficial for battery-powered devices, as the battery replacement frequency is reduced. The above experimental results revealed that mechanical pressure

could affect the electrochemical reactions that occur inside batteries.

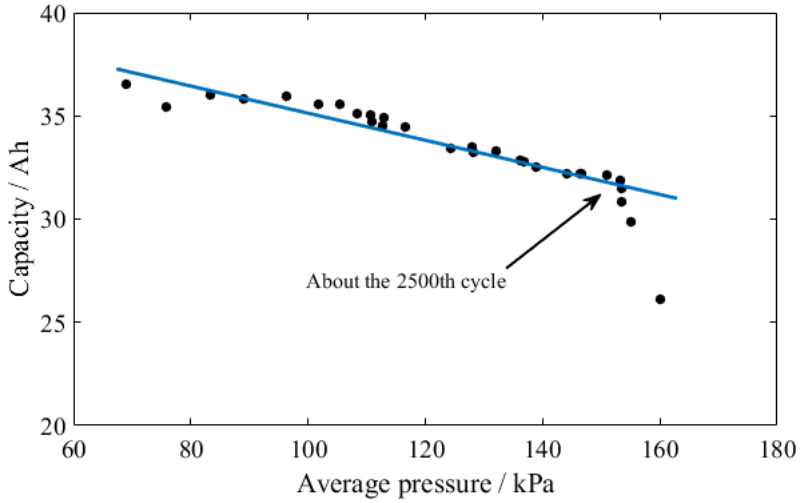

Figure 5. Battery capacity vs. average pressure during charge-discharge cycles.

Fig. 5 presents the capacity vs. pressure curve of the constrained battery during the charge-discharge cycles. The battery capacity decreased quickly and approximately linearly as the battery pressure increased during the first 2500 charge-discharge cycles. Similar results were reported by Cannarella and Arnold [29]. Moreover, as mentioned in section 3.1, the increase in battery pressure was caused by growth of the SEI film. Therefore, it could be deduced that the decrease in battery capacity observed in this stage was mainly due to growth of the SEI film.

The capacity of the unconstrained battery decreased rapidly during the late charge-discharge cycling stages (after 2100 charge-discharge cycles), whereas the capacity of the constrained battery was still relatively high until approximately the 2500th charge-discharge cycle, when it began to decrease. However, the pressure on the battery surface still increased steadily during this process (Fig. 3 (b)). After approximately 2500 cycles, the relationship between the capacity decay and pressure increase was no longer linear, which indicated that during the late charge-discharge cycling stages, factors other than growth of the SEI film presented a predominant effect on battery aging. It is worth noting that the capacity of the constrained battery suddenly dropped significantly at approximately the 3100th cycle, indicating that major problems, such as electrode material damage, may have occurred inside the battery.

To further investigate the causes of constrained battery failure and the effect of external pressure on battery aging during the late charge-discharge cycling stages, the batteries tested in this study were disassembled after the cycling tests, and their internal components were analyzed by using SEM.

Fig. 6 presents SEM images of the anodes and cathodes of the constrained and unconstrained batteries. The ternary cathode material exhibited a closely packed, crystalline microstructure (Fig. 6 (a), (b), (c) and (d)). The figures show that the constrained cathode particles had signs of destruction compared to the unconstrained cathode particles, as shown by the white arrows, although the phenomenon was not very obvious. The anodes consisted of layers of graphite, and the anode surface of the constrained battery was coarser than that of the unconstrained battery (Fig. 6 (e) and (g)). Some cracks were identified on the anode surface of the constrained battery, and a magnified image is

presented in Fig. 6 (h).

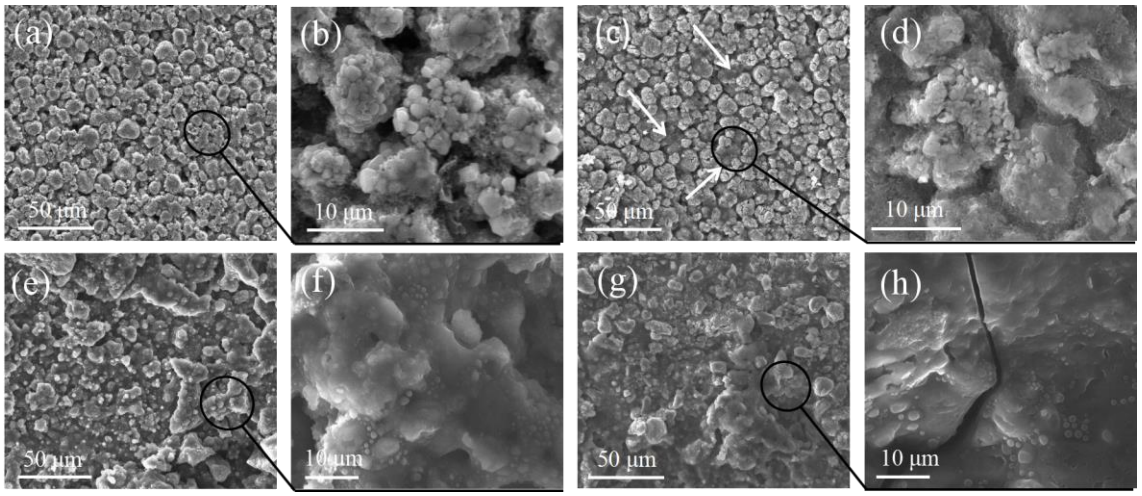

Figure 6. Scanning electron microscopy images of constrained and unconstrained batteries: (a) and (b) cathode surfaces of the unconstrained battery, (c) and (d) cathode surfaces of the constrained battery, (e) and (f) anode surfaces of the unconstrained battery, (g) and (h) anode surfaces of the constrained battery.

The differences observed between the electrode surfaces of the constrained and unconstrained batteries were likely attributable to the external pressure, particularly during the late cycling stages. The capacity curves of the two batteries were not significantly different in the early stages, which indicated that cracks on the anode surfaces and particle destruction on the cathode of the constrained battery formed during the late cycling stages. The electrode material exposed via the cracks could react with the electrolyte, leading to further consumption of recyclable lithium. Once formed, the anode cracks rapidly extended owing to electrochemical corrosion, which accelerated the aging of the electrode material and consequently resulted in the rapid decrease in battery capacity [30]. At the same time, the dissolved cathode particles would also undergo side reactions with the electrolyte, producing CO2 and other gases, accelerating the loss of recyclable lithium [8]. The appearance of anode cracks was likely the reason for the sudden drop in the capacity of the constrained battery at approximately 3100 cycles (Fig. 4). However, the external pressure of the battery did not increase suddenly due to the formation of the anode cracks, indicating that the cracks did not contribute much to an increase in stress in the vertical direction.

The reasons for the surface differences between the two battery electrodes could be inferred as follows. The pressure distribution on the surface of the fixed compressed battery was not uniform during charge-discharge cycling [9, 22]. This was likely attributed to the different amounts of lithium ions embedded at different sites. Because of the limitations of the current processing technology, the coating of electrode material on both the anode and cathode plates was not uniform. Owing to the embedding and releasing of lithium ions, the stress distribution on the battery surface was nonuniform, which promoted battery aging [31]. In return, when uneven aging occurred on the electrode surfaces, the uneven distribution of stress was accelerated. In short, owing to the irreversible accumulation of

stress in the battery during the late charge-discharge cycling stages, the pressure inside the battery significantly increased. Moreover, local stress accumulated because of the uneven coating of the electrode material, and the risk of fatigue failure of the electrode material increased after more than 3000 charge-discharge cycles. The combination of all these factors led to the formation of cracks on the anode surface and particle destruction on the cathode surface.

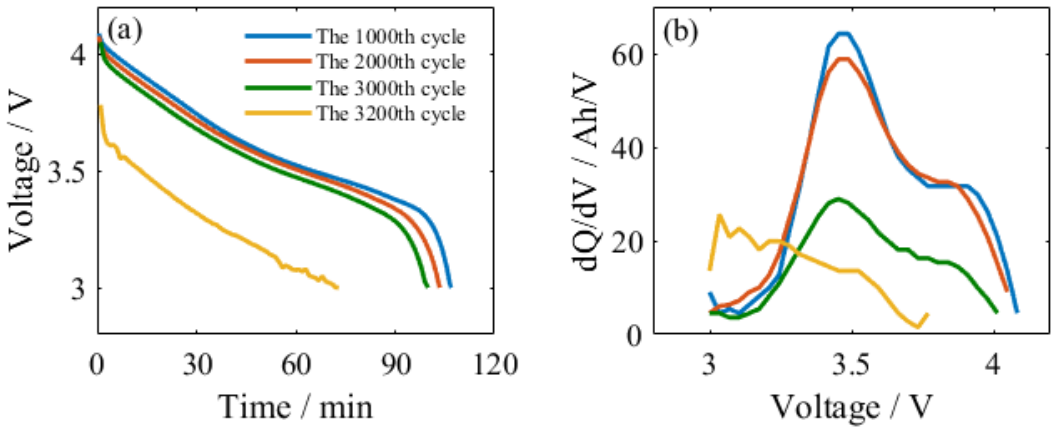

Figure 7. Aging analysis curves of the constrained battery: (a) voltage discharge curves, and (b) incremental capacity (IC) curves.

Incremental capacity analysis (ICA) is an important method for exploring battery aging [32, 33]. To more deeply explore the aging mechanism of the constrained battery during the late cycling stages, voltage discharge curves and incremental capacity (IC) curves of four different stages are drawn in Fig. 7. Because constant-current constant-voltage charging and constant-current discharging were used in this paper and the sampling period of the device was set to 30 s, the discharge curves were used for ICA. Although accuracy was difficult to guarantee, qualitative analysis could be performed. As illustrated in Fig. 7 (a), the discharge voltage of the battery gradually decreased as the cycle number increased. At the 3200th cycle, the voltage discharge curve had lost its original characteristics, indicating that the electrode active material of the battery had been severely damaged. The same phenomenon also occurred in the IC curves. As illustrated in Fig. 7 (b), the 3200th IC curve was severely deformed, which meant that severe damage had occurred in the electrode active material of the battery. Moreover, the 3000th IC curve had significantly degraded compared with the 1000th and 2000th cycles, indicating that there was loss of active material, which corresponded to the decay curve in Fig. 4.

The above analysis results were consistent with the SEM results. That is, the sudden decrease in capacity at approximately 3100 cycles was most likely caused by the severe destruction of the electrode material. These results also showed that after more than 3000 charge-discharge cycles, the relatively large external pressure was detrimental to battery life.

3.3 Effect of pressure on battery aging

A schematic diagram of the effect of pressure on aging is illustrated in Fig. 8. Side reactions occurred inside the batteries during cycling, which consumed the electrolyte and generated bubbles.

These reactions resulted in loss of contact between the internal components of the battery, such as the fuchsia-colored areas in Fig. 8, which further generated excessive local currents and caused lithium plating and consequently accelerated battery aging [31, 34]. The unconstrained battery in our study could undergo lithium plating during the late cycling stages owing to the significant consumption of its electrolyte, but this was not the focus of this article, and we will not discuss it much here. An external pressure could allow the generated bubbles to migrate toward the edge of the battery, which could improve the contact efficiency and reduce the occurrence of lithium plating. Moreover, an external pressure could reduce the ohmic resistance, which was beneficial for the battery cycle life [20, 21]. Therefore, when the capacity of the unconstrained battery decreased rapidly, the constrained battery still had good cycling performance.

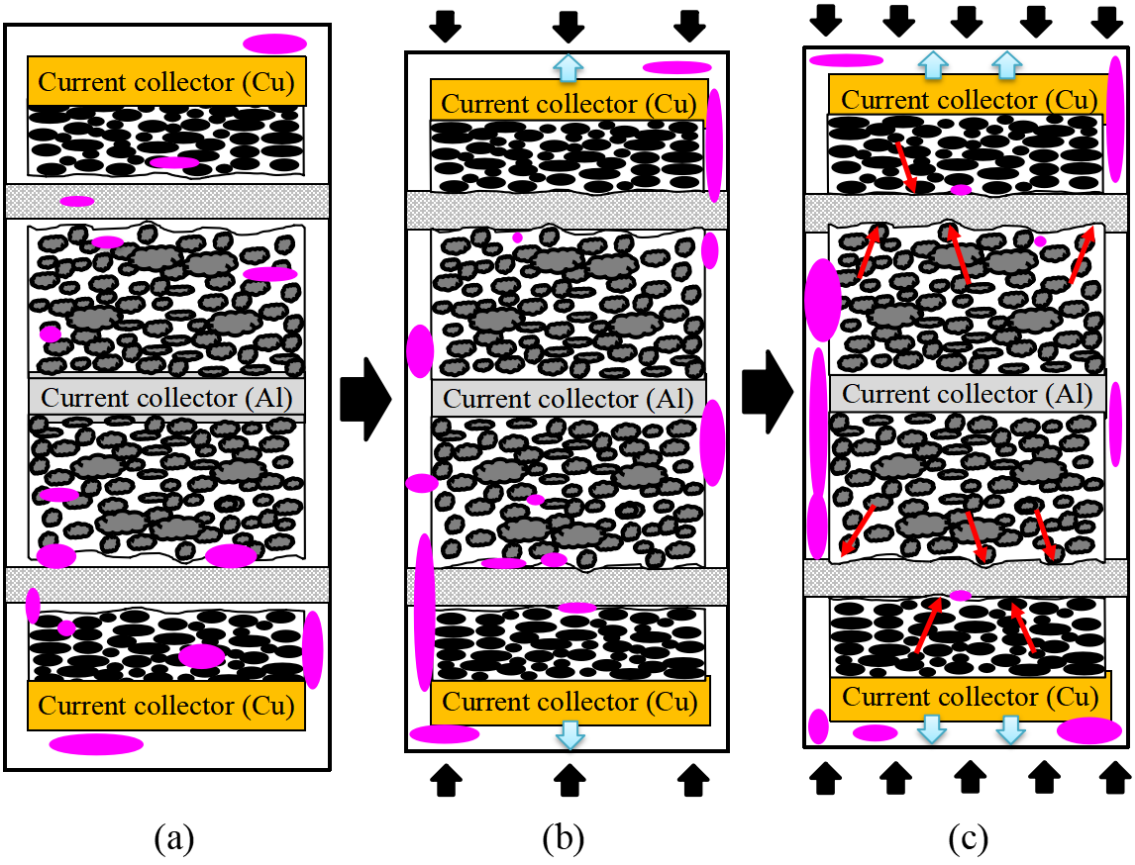

Figure 8. Schematic diagram of the effect of pressure on battery aging: (a) unconstrained battery, (b) early cycling stages of a constrained battery, and (c) late cycling stages of a constrained battery.

However, as depicted in Fig. 3 (b), internal stress accumulated irreversibly in the battery during cycling, and therefore, the battery was subjected to a higher pressure during late charge-discharge cycles. In this study, the pressure during the late charge-discharge cycles was approximately 2.7 times that during the initial charge-discharge cycle, and the pressure would be higher if the battery was in the charged state. This high pressure would cause the separator to deform and, in turn, hinder the transport of lithium ions and adversely affect the battery [10, 18]. Moreover, as mentioned in section 3.2, the electrode surfaces were not flat owing to the limitations in the processing technology. Consequently,

nonuniform stress always accumulated on electrode surfaces when an external pressure was applied to the battery. During the early cycling stages, the effect of the external pressure was positive rather than negative, and thus, the constrained battery presented good cycling characteristics. However, the risk of fatigue failure of the electrode material increased after thousands of charge-discharge cycles. The negative effect of the external pressure also increased with cycling and could become dominant during the late cycling stages; therefore, the electrodes would likely undergo cracking and destruction in areas subjected to excessively high pressure during the late cycling stages, as indicated by the red arrows in Fig. 8.

3.4 Verification test

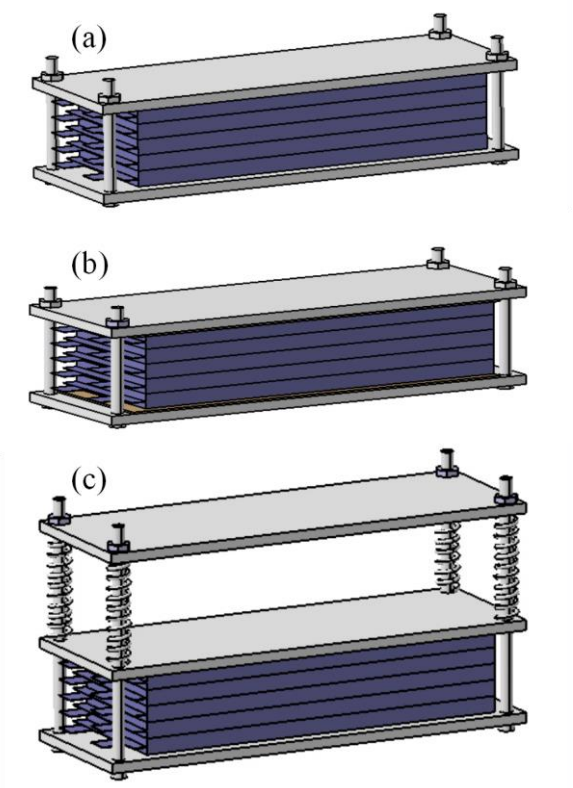

Figure 9. Three different constraint methods: (a) direct use of steel plates, (b) placement of silicone pads between the battery pack and steel compression plates, and (c) use of springs.

To confirm the above conclusion on the negative effect of irreversible stress accumulation on anode and cathode materials under the fixed constraint, battery pressure tests were conducted using different constraint schemes. To shorten the duration of the experiments, three groups of test battery packs were investigated, and each group consisted of five 10 Ah commercial batteries identical to those used for the previous experiment. However, the difference lay in the use of the winding process. The batteries in group (a) were directly constrained using steel plates, those in group (b) were constrained by placing 0.7 mm thick silicone pads with a maximum compression of 0.2 mm each between the steel plates and battery pack, and those in group (c) were constrained using springs. These constraint schemes simulated the working environment of the batteries in use because batteries are

usually used in packs and are limited by the pack volume, so it is difficult to keep outer cells and inner cells at the same pressure. The batteries were cycled with a parallel connection, and the initial pressure was set to be 69 kPa for each battery pack. The same charging-discharging protocol was applied to each battery pack, namely, CCCV charging at 0.5 C and a cutoff voltage of 4.2 V followed by CC discharging at 0.5 C and a cutoff voltage of 3.0 V. Ten-minute intervals were allowed between charging and discharging. A schematic diagram of the experimental setup is presented in Fig. 9.

Hooke's law can be written as F = k × x, where F and k are the force and elasticity coefficient, respectively, and x is the increase in the volume of the batteries during cycling in this study. The first group of batteries was subjected to a rigid constraint with a very large k value, and thus, the battery thickness could be considered to be constant. The silicone pads used to constrain the batteries in the second group allowed for a certain level of elastic compression, and thus, k was relatively large. However, the constraint became rigid when the compression exceeded 0.2 mm. Compared to the k values of the batteries in groups (a) and (b), that of the batteries in group (c) was smaller, and the expansion and contraction of the springs during the charge-discharge process stabilized the mechanical pressure on the batteries. We qualitatively analyzed the effect through the three different sets of constraint schemes.

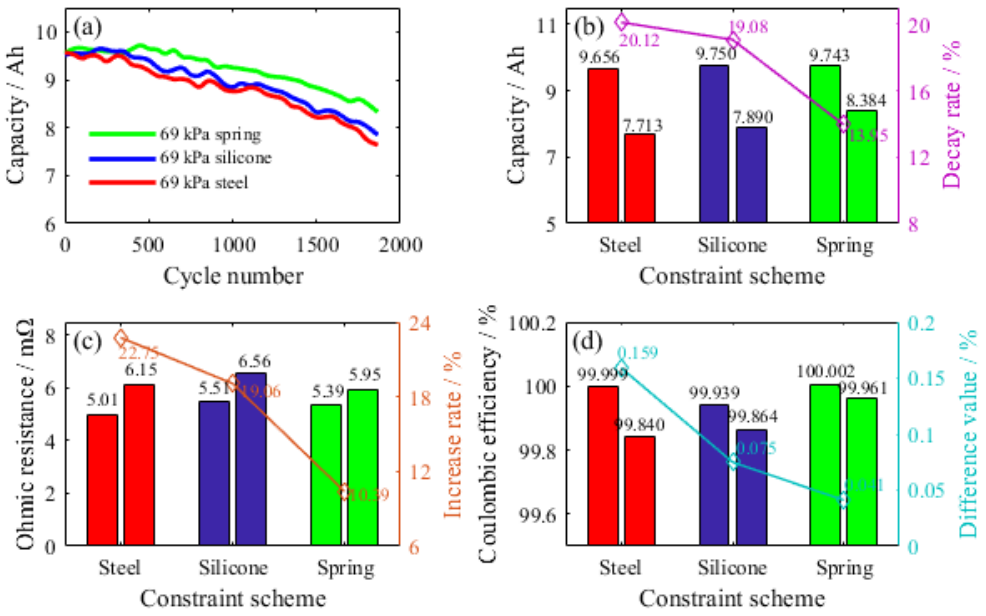

Figure 10. Comparison of aging results of the three groups: (a) decay curves of the average capacity in the three battery packs, (b) comparison of the capacity decrease rates of the battery packs, (c) comparison of the ohmic resistance increase rates of the battery packs, and (d) comparison of the coulombic efficiencies of the battery packs. Each constraint mode contains two bars of the same color, with the left representing the values at the beginning of the experiment and the right representing the values at the end of the experiment.

Fig. 10 (a) presents the changes in the average capacity of the batteries of each group during cycling for the first 1866 charge-discharge cycles. The results indicated that the batteries in the spring group presented the best cycling performance, while those in the steel plate group presented the worst cycling performance of all groups. No significant differences were observed in the cycling performance of the batteries in the three groups over the first approximately 400 charge-discharge

cycles. However, as cycling continued, the internal stress continued to accumulate, and the performance of the batteries in the spring group exceeded those of the batteries in the other groups.

The average capacities over the first and last 10 charge-discharge cycles were considered to be the initial and residual capacities, respectively, for all groups of batteries. The capacity decrease rates over the first 1866 charge-discharge cycles for the batteries in the three groups are summarized in Fig. 10 (b).

As illustrated in Fig. 10 (b), the capacity decrease rate for the batteries in the spring group was 5.13% and 6.17% lower than those of the batteries in the steel plate and silicone pad groups, respectively, which indicated that the spring constraint was more favorable for extending the battery cycle life.

The average ohmic resistance before cycling was considered to be the initial ohmic resistance, and the average ohmic resistance after cycling was considered to be the final ohmic resistance. The ohmic resistance increase rates of the three groups of batteries are shown in Fig. 10 (c). As illustrated in Fig. 10 (c), the ohmic resistance increase rate for the batteries in the spring group was 8.67% and 12.36% lower than those of the batteries in the steel plate and silicone pad groups, respectively. A lower ohmic resistance can reduce the internal loss during battery discharge, so the spring constraint was more favorable for battery discharge performance.

The coulombic efficiency was compared in the same way as the ohmic resistance above. Fig. 10 (d) illustrates the three groups of coulombic efficiencies before and after cycling. The spring constraint group still had a higher coulombic efficiency than the other groups at the end of the cycling, which meant that the spring constraint scheme had a higher energy conversion efficiency and a more stable internal environment.

As mentioned in section 3.3, the battery under the fixed constraint suffered increasing external pressure, and the ability to work under pressure decreased as the cycling progressed. Unlike the other two constraints, the spring constraint always maintained the external pressure in the vicinity of the proper level, which not only improved the contact efficiency inside the batteries and reduced the ohmic resistance but also absorbed the volume expansion caused by aging of the batteries and reduced the stress on both the anode and cathode surfaces. At the same time, the spring constraint reduced the negative effect of the uneven pressure distribution in the late stage of the cycling, so the spring constraint had the best results among the three groups not only in capacity but also in ohmic resistance and coulombic efficiency.

4. CONCLUSION

The expansion and contraction of the anode and the irreversible growth of the SEI film during charge-discharge cycling result in pressure changes on fixed batteries. External pressure could improve the contact efficiency of the electrode material, and proper external pressure is beneficial for the cycle life of lithium-ion batteries. The cycle life of lithium-ion battery in this paper could be extended by 400 charge-discharge cycles in the presence of an initial external pressure of 69 kPa. However, the increase of battery pressure in the late stage is unfavorable to the battery cycle life. In this paper, the external pressure of the fixed-constrained battery in the later stage is about 2.7 times that of the initial pressure.

After more than 3000 cycles, the battery capacity suddenly dropped. SEM and ICA results show that this is caused by the damage of the active material inside the battery, indicating that a relatively large external pressure is detrimental to battery life.

In order to reduce the negative effects of pressure increase on constrained battery, the comparative experiment was set. The comparative experiments revealed that when the number of charge-discharge cycles exceeded 1866, the capacity decrease rate for the batteries in the spring group was 5.13% and 6.17% lower than those of the batteries in the steel plate and silicone pad groups, respectively. The ohmic resistance increase rate for the batteries in the spring group was 8.67% and 12.36% lower than those of the batteries in the steel plate and silicone pad groups, respectively. The spring constraint group still had a higher coulombic efficiency than the other groups at the end of the cycling. These occurred because springs could absorb the volume expansion of batteries and maintained the external pressure relatively constant. Therefore, an appropriate elastic constraint can maximize the cycle life of the battery.

ACKNOWLEDGEMENTS
The research presented within this paper is supported by the Hunan Fengyuan Yeshine Kingco New Energy Co., Ltd. Furthermore, the authors are thankful to the company managers for their equipment support and valuable advice.

References

1. B. Scrosati and J. Garche, *J. Power Sources*, 195 (2010) 2419.
2. L. Su, J. Zhang, C. Wang, Y. Zhang, Z. Li, Y. Song, T. Jin and Z. Ma, *Appl. Energy*, 163 (2016) 201.
3. J. Wang, P. Liu, J. Hicks-Garner, E. Sherman, S. Soukiazian, M. Verbrugge, H. Tataria, J. Musser and P. Finamore, *J. Power Sources*, 196 (2011) 3942.
4. T. G. Zavalis, M. Klett, M. H. Kjell, M. Behm, R. W. Lindström and G. Lindbergh, *Electrochim. Acta*, 110 (2013) 335.
5. X. Feng, D. Ren, S. Zhang, X. He, L. Wang and M. Ouyang, *Int. J. Electrochem. Sci*., 14 (2019) 44.
6. Q. Lu, P. Lian, Q. Wang, Z. Zuo and Y. Mei, *Int. J. Electrochem. Sci*., 14 (2019) 10270.
7. Y. Gao, X. Zhang , J. Yang, B. Guo and X. Zhou, *Int. J. Electrochem. Sci.*, 14 (2019) 3180.
8. J. Vetter, P. Novák, M. R. Wagner, C. Veit, K. C. Möller, J. O. Besenhard, M. Winter, M. Wohlfahrt-Mehrens, C. Vogler and A. Hammouche, *J. Power Sources*, 147 (2005) 269.
9. A. Barai, R. Tangirala, K. Uddin, J. Chevalier, Y. Guo, A. McGordon and P. Jennings, *J. Energy Storage*, 13 (2017) 211.
10. J. Cannarella and C. B. Arnold, *J. Power Sources*, 226 (2013) 149.
11. J. Cannarella and C. B. Arnold, *J. Power Sources*, 245 (2014) 745.
12. L. Zhou, L. Xing, Y. Zheng, X. Lai, J. Su, C. Deng and T. Sun, *Int. J. Energ. Res*., (2020) 1.
13. A. S. Mussa, M. Klett, G. Lindbergh and R. W. Lindström, *J. Power Sources*, 385 (2018) 18.
14. B. Chen, J. Zhou, X. Pang, P. Wei, Y. Wu and K. Deng, *RSC Adv*., 4 (2014) 21072.
15. J. Christensen and J. Newman, *J. Solid State Electrochem*., 10 (2006) 293.
16. R. Fu, M. Xiao and S.-Y. Choe, *J. Power Sources*, 224 (2013) 211.
17. D. Liu, Y. Wang, Y. Xie, L. He, J. Chen, K. Wu, R. Xu and Y. Gao, *J. Power Sources*, 232 (2013) 29.
18. C. Peabody and C. B. Arnold, *J. Power Sources*, 196 (2011) 8147.
19. Y. S. C. J.S. Gnanaraj, M.D. Levi, D. Aurbach, *J. Electroanal. Chem*., 516 (2001) 89.

20. G. Berckmans, L. De Sutter, M. Marinaro, J. Smekens, J. Jaguemont, M. Wohlfahrt-Mehrens, J. van Mierlo and N. Omar, *Electrochim. Acta*, 306 (2019) 387.
21. V. Müller, R.-G. Scurtu, M. Memm, M. A. Danzer and M. Wohlfahrt-Mehrens, *J. Power Sources*, 440 (2019) 227148.
22. V. Müller, R.-G. Scurtu, K. Richter, T. Waldmann, M. Memm, M. A. Danzer and M. Wohlfahrt-Mehrens, *J. Electrochem. Soc*., 166 (2019) A3796.
23. J. Zhang, X. Han, C. Hu, H. Zhang and L. Zhang, *Automotive Engineering*, 38 (2016) No.6.
24. Y. Koyama, I. Tanaka, H. Adachi, Y. Makimura and T. Ohzuku, *J. Power Sources*, 119-121 (2003) 644.
25. J. R. Dahn, *Phys. Rev.* B, 44 (1991) 9170.
26. G. Kirczenow, *Phys. Rev. Lett*., 55 (1985) 2810.
27. A. J. Louli, L. D. Ellis and J. R. Dahn, *Joule*, 3 (2019) 745.
28. B. Bitzer and A. Gruhle, *J. Power Sources*, 262 (2014) 297.
29. J. Cannarella and C. B. Arnold, *J. Power Sources*, 269 (2014) 7.
30. R. Xu and K. Zhao, *J. Electrochem. Energy Convers. Storage*, 13 (2016) 030803.
31. T. C. Bach, S. F. Schuster, E. Fleder, J. Müller, M. J. Brand, H. Lorrmann, A. Jossen and G. Sextl, *J. Energy Storage*, 5 (2016) 212.
32. X. Feng, C. Weng, X. He, L. Wang, D. Ren, L. Lu, X. Han and M. Ouyang, *Energies*, 11 (2018) 2323.
33. X. Han, M. Ouyang, L. Lu, J. Li, Y. Zheng and Z. Li, *J. Power Sources*, 251 (2014) 38.
34. T. Guan, S. Sun, F. Yu, Y. Gao, P. Fan, P. Zuo, C. Du and G. Yin, *Electrochim. Acta*, 279 (2018) 204

© 2020 The Authors. Published by ESG (www.electrochemsci.org). This article is an open access article distributed under the terms and conditions of the Creative Commons Attribution license (http://creativecommons.org/licenses/by/4.0/).